Autonomous Exploration, Reconstruction, and Surveillance of 3D Environments Aided by Deep Learning

Preprint · September 2018

DOI: 10.48550/arXiv.1809.06025

2 authors, including:

Richard Tsai
University of Texas at Austin
147 PUBLICATIONS **4,205** CITATIONS

SEE PROFILE

Autonomous Exploration, Reconstruction, and Surveillance of 3D Environments Aided by Deep Learning

Louis Ly[1] and Yen-Hsi Richard Tsai[1]

***Abstract*— We propose a greedy and supervised learning approach for visibility-based exploration, reconstruction and surveillance. Using a level set representation, we train a convolutional neural network to determine vantage points that maximize visibility. We show that this method drastically reduces the on-line computational cost and determines a small set of vantage points that solve the problem. This enables us to efficiently produce highly-resolved and topologically accurate maps of complex 3D environments. Unlike traditional next-best-view and frontier-based strategies, the proposed method accounts for geometric priors while evaluating potential vantage points. While existing deep learning approaches focus on obstacle avoidance and local navigation, our method aims at finding near-optimal solutions to the more global exploration problem. We present realistic simulations on 2D and 3D urban environments.**

I. INTRODUCTION

We consider the problem of generating a minimal sequence of observing locations to achieve complete line-of-sight visibility coverage of an environment. If the environment is initially unknown, the problem is called exploration and reconstruction. This is particularly useful for autonomous agents to map out unknown, or otherwise unreachable environments, such as undersea caverns. If the environment is known, the problem is one of surveillance: *how should a minimal set of sensors be placed to maintain complete surveillance of an environment?*

A. PROBLEM FORMULATION

Let X be the set consisting of all possible environment configurations. Each $\Omega \in X$ is an open set representing the free space and Ω^c is the set of obstacles. Let $\mathcal{P}_{x_i}\Omega$ be the projection of Ω along each vantage point x_i. That is, $\mathcal{P}_{x_i}\Omega$ is a set of range measurements defined on the unit sphere. The back projection $\mathcal{Q}$ maps the range measurements to the visibility set $\mathcal{V}_{x_i}\Omega := \mathcal{Q}(\mathcal{P}_{x_i})\Omega$; points in this set are visible from x_i. As more range measurements are acquired, Ω can be approximated by the *cumulatively visible set* Ω_k:

$$\Omega_k = \bigcup_{i=0}^{k} \mathcal{V}_{x_i}\Omega$$

By construction, Ω_k admits partial ordering: $\Omega_{i-1} \subset \Omega_i$. For suitable choices of x_i, it is possible that $\Omega_n \to \Omega$ (say, in the Hausdorff distance).

We aim at determining a *minimal set of vantage points* from which every $x \in \Omega$ can be seen. One may formulate a constrained optimization problem and look for sparse solutions in the following context. Let $D \subset \mathbb{R}^d$, $d = 2, 3$, be the bounded cubic region. Let I be a real valued function defined on a grid over D, with m nodes in each dimension. The constrained optimization problem is:

$$\min_{I:\mathbb{R}^{m^d}\mapsto\{0,1\}} ||I||_0 \quad \text{subject to} \quad \bigcup_{\{x|I(x)=1\}} \mathcal{V}_x\Omega = \Omega. \quad (1)$$

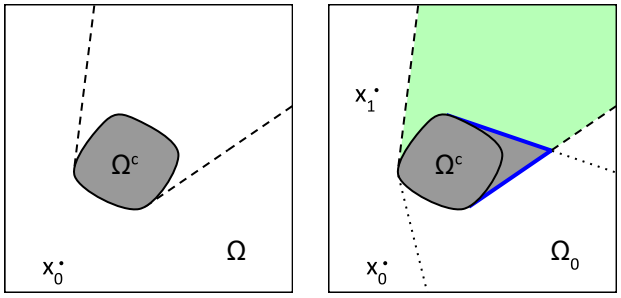

Fig. 1: An illustration of the environment. Dashed and dotted lines are the horizons from x_0 and x_1, respectively. Their shadow boundary, B_1, is shown in thick, solid blue. The area of the green region represents $g(x_1; \Omega_0, \Omega)$.

B. A GREEDY APPROACH

We propose a greedy approach which sequentially determines a new vantage point, x_{k+1}, based on the information gathered from all previous vantage points, $x_0, x_1, \cdots, x_k$. The strategy is greedy because x_{k+1} would be a location that *maximizes the information gain*.

For the surveillance problem, the environment Ω is known. We define the *gain* function:

$$g(x; \Omega_k, \Omega) := |\mathcal{V}_x\Omega \cup \Omega_k| - |\Omega_k|, \quad (2)$$

i.e. the volume of the region that is visible from x but not from $x_0, x_1, \cdots, x_k$. The next vantage point should be chosen to maximize the newly-surveyed area:

$$x_{k+1} = \arg\max_{x\in\Omega} g(x; \Omega_k, \Omega). \quad (3)$$

The problem of exploration is even more challenging since, by definition, the environment is not known. However, we remark that in practice, one is typically interested only in a subset S of all possible environments X. For example, cities generally follow a grid-like pattern. Knowing these priors can help guide our estimate of g for certain types of Ω, even when Ω is unknown initially.

We propose to encode these priors formally into the parameters, θ, of a learned function:

$$g_\theta(x; \Omega_k, B_k) \text{ for } \Omega \in S,$$

[1] Oden Institute for Computational Engineering and Sciences, The University of Texas at Austin {louis,ytsai}@ices.utexas.edu

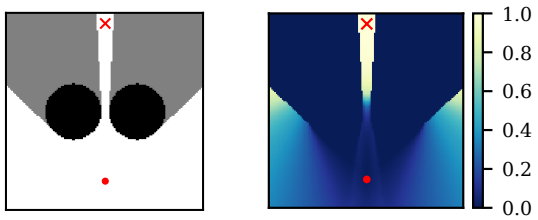

Fig. 2: Left: the map of a scene consisting of two disks. Right: the intensity of the corresponding gain function. The current vantage point is shown as the red dot. The location which maximizes the gain function is shown as the red x.

where B_k is the part of $\partial\Omega_k$ that may actually lie in the free space Ω. More precisely, $B_k = \partial\Omega_k \backslash \Omega^c$.

See Figure 2 for an example gain function. We shall demonstrate that while training for g_θ, incorporating the shadow boundaries helps, in some sense, localize the learning of g, and is essential in creating usable g_θ.

II. RELATED WORKS

The surveillance problem is related to the art gallery problem in computational geometry, where the task is to determine the minimum set of guards who can together observe a polygonal gallery. Vertex guards must be stationed at the vertices of the polygon, while point guards can be anywhere in the interior. For simply-connected polygonal scenes, Chvátal showed that $\lfloor n/3 \rfloor$ vertex guards, where n is the number of vertices, are sometimes necessary and always sufficient [6]. For polygonal scenes with h holes, $\lfloor (n+h)/3 \rfloor$ point guards are sufficient [5], [12]. However, determining the optimal set of observers is NP-complete [31], [21], [17].

Goroshin et al. propose an alternating minimization scheme for optimizing the visibility of N observers [10]. Kang et al. use a system of differential equations to optimize the location and orientation of N sensors to maximize surveillance [13]. Both works assume the number of sensors is given.

For the exploration problem, a class of approaches pick new vantage points along shadow boundaries (aka frontiers), the boundary between free and occluded regions [33]. Ghosh et al. propose a frontier-based approach for 2D polygonal environments which requires $r + 1$ views, where r is the number of reflex angles [8]. For general 2D environments, Landa et al. [16], [14], [15] use high order ENO interpolation to estimate curvature, which is then used to determine how far past the horizon to step. However, it is not necessarily optimal to pick only points along the shadow boundary, e.g. when the map is a star-shaped polygon [8].

Next-best-view algorithms try to find vantage points that maximize a utility function, consisting of some notion of *information gain* and another criteria such as path length. The vantage point does not have to lie along the shadow boundary. A common measure of information gain is the volume of *entire* unexplored region within sensor range that is not occluded by obstacles [9], [3], [4], [11]. Surmann et al. count the number of intersections of rays into the occlusion [26], while Valente et al. [32] use the surface area of the shadow boundary, weighted by the viewing angle from the vantage points, to define potential information gain. The issue with these heurisitics is that they are independent of the underlying geometry. In addition, computing the information gain at each potential vantage point is costly and another heurisitic is used to determine which points to sample.

There has been some attempts to incorporate deep learning into the exploration problem, but they are myopic and focus on navigation rather than exploration. The approach of Bai et al. [1] terminates when there is no occlusion within view of the agent, even if the global map is still incomplete. Tai and Liu [27], [28], [18] train agents to learn obstacle avoidance.

Our work uses a gain function to steer a non-myopic greedy approach, similar to the next-best-view algorithms. However, our measure of information gain takes the geometry of the environment into account. By taking advantage of precomputation via convolutional neural networks, our model learns shape priors for a large class of obstacles and is efficient at runtime. We use a volumetric representation which can handle arbitrary geometries in 2D and 3D. Also, we assume that the sensor range is larger than the domain, which makes the problem more global and challenging.

III. METHODOLOGY

Given the set of previously-visited vantage points, we compute the cumulative visibility and shadow boundaries. We approximate the gain function by applying the trained neural network on this pair of inputs, and pick the next point according to (3). This procedure repeats until there are no shadow boundaries or occlusions.

The data needed for the training and evaluation of g_θ are computed using level sets [23], [25], [22]. Occupancy grids may be applicable, but we choose level sets since they have proven to be accurate and robust. In particular, level sets are necessary for subpixel resolution of shadow boundaries and they allow for efficient visibility computation, which is crucial when generating the library of training examples.

The training geometry is embedded by a level set function, denoted by ϕ. For each vantage point x_i, the visibility set is represented by the level set function ψ_{x_i}, which is computed efficiently using the algorithm described in [29].

In the calculus of level set functions, unions and intersections of sets are translated, respectively, into taking maximum and minimum of the corresponding characteristic functions. The cumulatively visible sets Ω_k are represented by the level set function $\Psi_k(x)$, which is defined recursively by $\Psi_k = \max(\Psi_{k-1}, \psi_{x_k})$, point-wise, with $\Psi_0 = \psi_{x_0}$.

Thus we have $\Omega = \{\phi > 0\}$, $\mathcal{V}_{x_i}\Omega = \{\psi_{x_i} > 0\}$, and $\Omega_k = \{\Psi_k > 0\}$. The shadow boundaries B_k are approximated by the "smeared out" delta function b_k:

$$b_k(x) := \delta_\varepsilon(\Psi_k) \cdot [1 - H(\delta_\varepsilon(\phi))], \tag{4}$$

where $\delta_\varepsilon(x) = \frac{2}{\varepsilon}\cos^2\left(\frac{\pi x}{\varepsilon}\right) \cdot \mathbb{1}_{[-\frac{\varepsilon}{2},\frac{\varepsilon}{2}]}(x)$, and $H(x)$ is the Heaviside function. In our implementation, we take $\varepsilon = 3\Delta x$ where Δx is the grid node spacing. We refer the readers to [30] for a short review of relevant details.

A. SURVEILLANCE

When the environment Ω is known, we can compute the gain function exactly

$$g(x;\Omega_k,\Omega) = \int H\Big(H\big(\psi_x(\xi)\big) - H\big(\Psi_k(\xi)\big)\Big)\, d\xi. \quad (5)$$

We remark that the integrand will be 1 where the new vantage point uncovers something not previously seen. Computing g for all x is costly; each visibility and volume computation requires $O(m^d)$ operations, and repeating this for all points in the domain results in $O(m^{2d})$ total flops. We approximate it with a function $\tilde{g}_\theta$ parameterized by θ:

$$\tilde{g}_\theta(x;\Psi_k,\phi,b_k) \approx g(x;\Omega_k,\Omega).$$

B. EXPLORATION

If the environment is unknown, we directly approximate the gain function by learning the parameters θ of a function

$$g_\theta(x;\Psi_k,b_k) \approx g(x;\Omega_k,\Omega)H(\Psi_k)$$

using only the observations as input. Note the $H(\Psi_k)$ factor is needed for collision avoidance during exploration because it is not known *a priori* whether an occluded location y is part of an obstacle or free space. Thus $g_\theta(y)$ must be zero.

C. TRAINING

Ω is randomly sampled from a library. For each Ω, a sequence of data pairs is generated and included into the training set $\mathcal{T}$:

$$\big(\{\Psi_k,b_k\}, g(x;\Omega_k,\Omega)H(\Psi_k)\big), \qquad k=0,1,2,\ldots.$$

The function g_θ is learned by minimizing the empirical loss across all data pairs for each Ω in the training set $\mathcal{T}$:

$$\underset{\theta}{\operatorname{argmin}}\ \frac{1}{N}\sum_{\Omega\in\mathcal{T}}\sum_{k} L\Big(g_\theta(x;\Psi_k,b_k), g(x;\Omega_k,\Omega)H(\Psi_k)\Big)$$

where N is the total number of data pairs. We use the cross entropy loss function:

$$L(p,q) = \int p(x)\log q(x) + (1-p(x))\log(1-q(x))\ dx$$

D. MODEL ARCHITECTURE

We use convolutional neural networks (CNNs) to approximate the gain function, which depends on the shape of Ω and the location x. CNNs have been used to approximate functions of shapes effectively in many applications. Their feedforward evaluations are efficient if the off-line training cost is ignored. The gain function $g(x)$ does not depend *directly* on x, but rather, x's visibility of Ω, with a domain of dependence bounded by the sensor range. So, we expect certain translation invariance in the computation of the gain function. We employ a fully convolutional approach for learning g, which makes the network applicable to domains of different sizes, with straight-forward generalization to 3D.

We base the architecture of the CNN on U-Net [24], which has had great success in dense inference problems, such as image segmentation. It aggregates information from various layers in order to have wide receptive fields while maintaining pixel precision. The main design choice is to make sure that the receptive field of our model is sufficient. That is, we want to make sure that the value predicted at each voxel depends on a sufficiently large neighborhood. For efficiency, we use convolution kernels supported in the 3^d-pixel set. By stacking multiple layers, we can achieve large receptive fields. Thus the complexity for feedforward computations is linear in the total number of grid points.

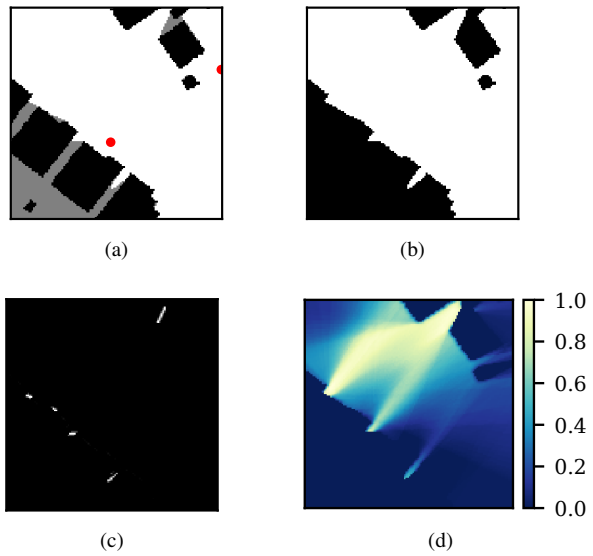

Fig. 3: A training data pair consists of the cumulative visibility and shadow boundaries as input, and the gain function as the output. a) The underlying map with current vantage points shown in red. b) The cumulative visibility of the current vantage points. c) The corresponding shadow boundaries. d) The corresponding gain function.

Define a *conv block* as the following layers: convolution, batch norm, leaky `relu`, stride 2 convolution, batch norm, and leaky `relu`. Each *conv block* reduces the image size by a factor of 2. The latter half of the network increases the image size using *deconv blocks*: bilinear 2x upsampling, convolution, batch norm, and leaky `relu`.

Our 2D network uses 6 *conv blocks* followed by 6 *deconv blocks*, while our 3D network uses 5 of each block. We choose the number of blocks to ensure that the receptive field is at least the size of the training images: 128×128 and $64\times64\times64$. The first *conv block* outputs 4 channels. The number of channels doubles with each *conv block*, and halves with each *deconv block*.

The network ends with a single channel, kernel of size 1 convolution layer followed by the sigmoid activation. This ensures that the network aggregates all information into a prediction of the correct size and range.

IV. EXPERIMENTS

We present some experiments to demonstrate the efficacy of our approach. Also, we demonstrate its limitations.

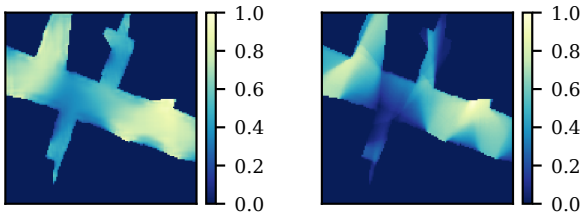

Fig. 4: Comparison of predicted (left) and exact (right) gain function for an Austin map. Although the functions are not identical, the predicted gain function peaks in similar locations to the exact gain function, leading to similar steps.

First, we train on 128×128 aerial city blocks cropped from INRIA Aerial Image Labeling Dataset [19]. It contains binary images with building labels from several urban areas, including Austin, Chicago, Vienna, and Tyrol. We train on all the areas except Austin, which we hold out for evaluation. We call this model **City-CNN**. We train a similar model **NoSB-CNN** on the same training data, but omit the shadow boundary from the input. Third, we train another model on synthetically-generated radial maps, such as the one in Figure 8. We call this model **Radial-CNN**.

Given a map, we randomly select an initial location. In order to generate the sequence of vantage points, we apply (3), using g_θ in place of g. Ties are broken by choosing the closest point to x_k. We repeat this process until there are no shadow boundaries, the gain function is smaller than ϵ, or the residual is less than δ, where the residual is defined as:

$$r = \frac{|\Omega \setminus \Omega_k|}{|\Omega|}. \tag{6}$$

We compare these against the algorithm which uses the exact gain function, which we call **Exact**. We also compare against **Random**, a random walker, which chooses subsequent vantage points uniformly from the visible region. We analyze the number of steps required to cover the scene and the residual as a function of the number of steps.

Lastly, we present a simulation for exploring a 3D urban environment. Due to the limited availability of datasets, the model, **3D-CNN**, is trained using synthetic $64 \times 64 \times 64$ voxel images consisting of tetrahedrons, cylinders, ellipsoids, and cuboids of random positions, sizes, and orientations. In the site[1], the interested reader may inspect the performance of the **3D-CNN** in some other challenging 3D environments.

For our experiments using trained networks, we make use of a CPU-only machine containing four Intel Core i5-7600 CPU @ 3.50GHz and 8 GB of RAM. Additionally, we use an Nvidia Tesla K40 GPU with 12 GB of memory for training and predicting the gain function in 3D scenes.

A. 2D CITY

The **City-CNN** model works well on 2D Austin maps. First, we compare the predicted gain function to the exact gain function on a 128×128 map, as in Figure 4. Without knowing the underlying map, it is difficult to accurately determine the gain function. Still, the predicted gain function peaks in locations similar to those in the exact gain function. This results in similar sequences of vantage points.

[1]http://visibility.page.link/demo

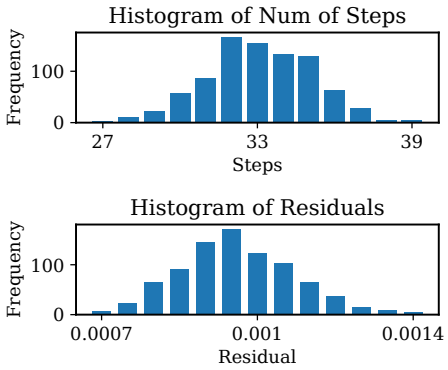

Fig. 5: Distribution of the residual and number of steps generated across multiple runs over an Austin map. The proposed method is robust against varying initial conditions. The algorithm reduces the residual to roughly 0.1 % within 39 steps by using a threshold on the predicted gain function as a termination condition.

The algorithm is robust to the initial positions. Figure 5 show the distribution of the number of steps and residual across over 800 runs from varying initial positions over a 512×512 Austin map. In practice, using the shadow boundaries as a stopping criteria can be unreliable. Due to numerical precision and discretization effects, the shadow boundaries may never completely disappear. Instead, the algorithm terminates when the maximum predicted gain falls below a certain threshold ϵ. In this example, we used $\epsilon = 0.1$. Empirically, this strategy is robust. On average, the algorithm required 33 vantage points to reduce the occluded region to within 0.1% of the total explorable area.

Figure 6a shows an example sequence consisting of 36 vantage points. Each subsequent step is generated in under 1 sec using the CPU and instantaneously with a GPU.

Even when the maximizer of the predicted gain function is different from that of the exact gain function, the difference in gain is negligible. This is evident when we see the residuals for **City-CNN** decrease at similar rates to **Exact**. Figure 7 demonstrates an example of the residual as a function of the number of steps for one such sequence generated by these algorithms on a 1024×1024 map of Austin. We see that **City-CNN** performs comparably to **Exact** approach in terms of residual. However, **City-CNN** takes 140 secs to generate 50 steps on the CPU while **Exact**, an $O(m^4)$ algorithm, takes more than 16 hours to produce 50 steps.

B. EFFECT OF SHADOW BOUNDARIES

The inclusion of the shadow boundaries as input to the CNN is critical for the algorithm to work. Without the shadow boundaries, the algorithm cannot distinguish between obstacles and occluded regions. If an edge corresponds to an

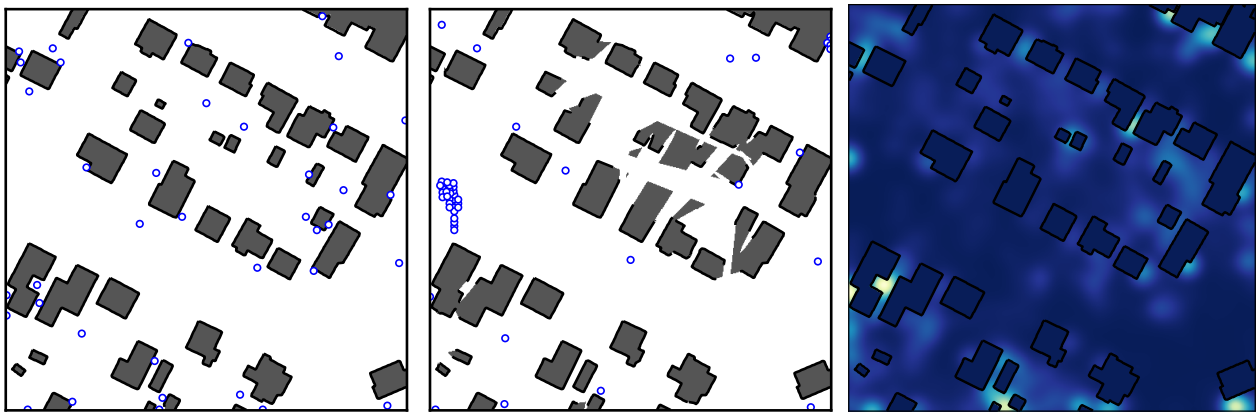

(a) (b) (c)

Fig. 6: Comparison of two models over a 512×512 Austin map. a) An example of 36 vantage points (blue disks) using **City-CNN** model. White regions are free space while gray regions are occluded. Black borders indicate edges of obstacles. b) A sequence of 50 vantage points generated from **NoSB-CNN**. The points cluster near flat edges due to ambiguity and the algorithm becomes stuck. Gray regions without black borders have not been fully explored. c) Distribution of vantage points generated by **City-CNN** method from various initial positions. Hot spots are brighter and are visited more frequently since they are essential for completing coverage.

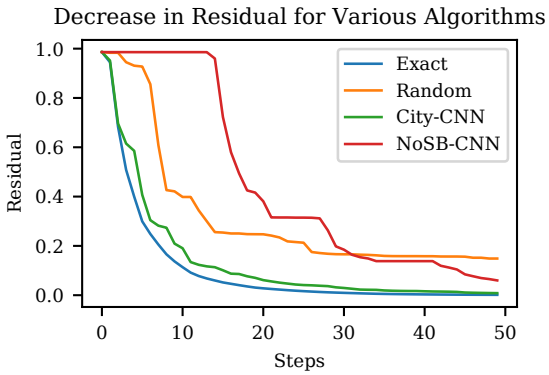

Fig. 7: Graph showing the decrease in residual over 50 steps among various algorithms starting from the same initial position for an Austin map. Without using shadow boundary information, **NoSB-CNN** can at times be worse than **Random**. Our **City-CNN** model is significantly faster than **Exact** while remaining comparable in terms of residual.

occluded region, then choosing a nearby vantage point will reduce the residual. However, choosing a vantage point near a flat obstacle will result in no change to the cumulative visibility. At the next iteration, the input is same as the previous iteration, and the result will be the same; the algorithm becomes stuck in a cycle. To avoid this, we prevent vantage points from repeating by zeroing out the gain function at that point and recomputing the argmax. Still, the vantage points tend to cluster near flat edges, as in Figure 6b. This clustering behavior causes the **NoSB-CNN** model to be, at times, worse than **Random**. See Figure 7 to see how the clustering inhibits the reduction in the residual.

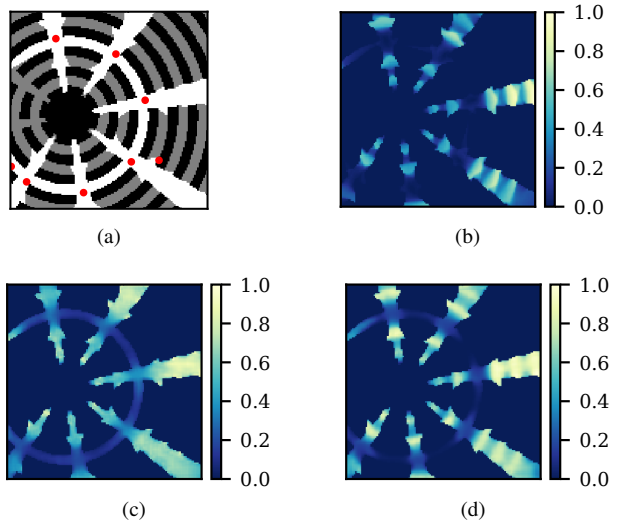

(a) (b) (c) (d)

Fig. 8: Comparison of gain functions produced with various models on a radial scene. Naturally, the CNN model trained on radial obstacles best approximates the true gain function. a) The underlying radial map with vantage points show in red. b) The exact gain function c) **City-CNN** predicted gain function. d) **Radial-CNN** predicted gain function.

C. EFFECT OF SHAPE

The shape of the obstacles, i.e. Ω^c, used in training affects the gain function predictions. Figure 8 compares the gain functions produced by **City-CNN** and **Radial-CNN**.

D. FREQUENCY MAP

Here we present one of our studies concerning the exclusivity of vantage point placements in Ω. We generated

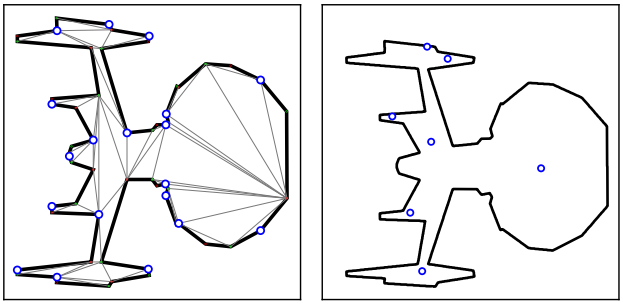

Fig. 9: Comparison of the computational geometry approach and the **City-CNN** approach to the art gallery problem. The blue circles are the vantage points computed by the methods. Left: A result computed by the computational geometry approach, given the environment. Right: An example sequence of 7 vantage points generated by the **City-CNN** model.

sequences of vantage points starting from over 800 different initial conditions using **City-CNN** model on a 512×512 Austin map. Then, we model each vantage point as a Gaussian with fixed width, and overlay the resulting distribution on the Austin map in Figure 6c. This gives us a frequency map of the most recurring vantage points. These hot spots reveal regions that are more secluded and therefore, the visibility of those regions is more sensitive to vantage point selection. The efficiency of the CNN method allows us to address many surveillance related questions for a large collection of relevant geometries.

E. ART GALLERY PROBLEM

Our proposed approach outperforms the computational geometry solution [20] to the art gallery problem, even though we do not assume the environment is known. The key issue with computational geometry approaches is that they are heavily dependent on the triangulation. In an extreme example, consider an art gallery that is a simple convex *n-gon*. Even though it is sufficient to place a single vantage point anywhere in the interior of the room, the triangulation-based approach produces a solution with $\lfloor n/3 \rfloor$ vertex guards.

Figure 9 shows an example gallery consisting of 58 vertices. The computational geometry approach requires $\lfloor \frac{n}{3} \rfloor = 19$ vantage points to completely cover the scene, even if point guards are used [5], [12]. The gallery contains $r = 19$ reflex angles, so the work of [8] requires $r+1 = 20$ vantage points. On average, **City-CNN** requires only 8 vantage points.

F. 3D ENVIRONMENT

We present a 3D simulation of a 250m$\times$250m environment based on Castle Square Parks in Boston. The map is discretized as a level set function on a $768 \times 768 \times 64$ voxel grid. At this resolution, small pillars are accurately reconstructed by our exploration algorithm. Each step can be generated in 3 seconds using the GPU or 300 seconds using the CPU. Parallelization of the distance function computation will further reduce the computation time significantly. A map of this size was previously unfeasible. See Figure 10 for snapshots of the algorithm in action. See Supplemental Material for a video clip of the exploration process.

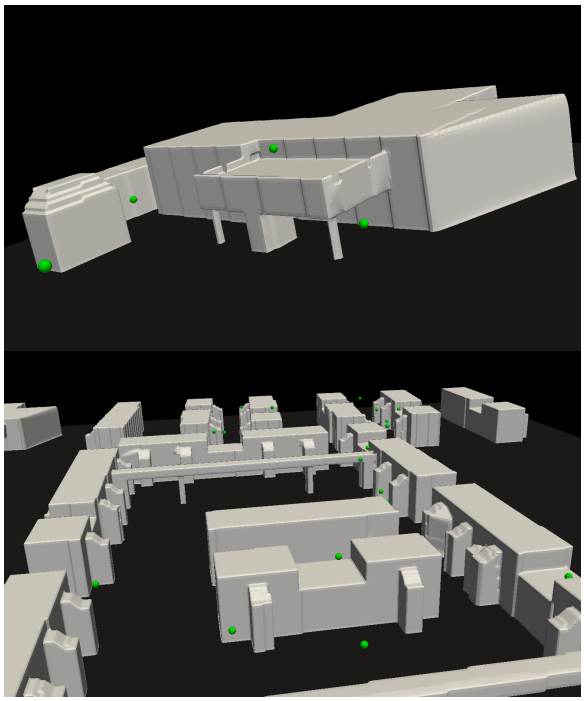

Fig. 10: Snapshots demonstrating the exploration of an initially unknown 3D urban environment using sparse sensor measurements. The green spheres indicate the vantage point. The gray surface is the reconstruction of the environment based on line of sight measurements taken from the sequence of vantage points. New vantage points are computed in virtually real time using **3D-CNN**.

V. CONCLUSION

From the perspective of inverse problems, we proposed a greedy algorithm for autonomous surveillance and exploration. We show that this formulation can be well-approximated using convolutional neural networks, which learns geometric priors for a large class of obstacles. The inclusion of shadow boundaries, computed using the level set method, is crucial for the success of the algorithm. One of the advantages of using the gain function (2), an integral quantity, is its stability with respect to noise in positioning and sensor measurements. In practice, we envision that it can be used in conjuction with SLAM algorithms [7], [2] for a wide range of real-world applications.

ACKNOWLEDGMENT

This work was partially supported by NSF Grant DMS-1720171. We thank Texas Advanced Computing Center (TACC) for providing the computational resources that made this work possible. Tsai also thanks National Center for Theoretical Sciences (NCTS) for hosting his visits to the center, where part of the research was being conducted.

REFERENCES

[1] S. Bai, F. Chen, and B. Englot. Toward autonomous mapping and exploration for mobile robots through deep supervised learning. In *2017 IEEE/RSJ International Conference on Intelligent Robots and Systems (IROS)*, pages 2379–2384. IEEE, 2017.

[2] T. Bailey and H. Durrant-Whyte. Simultaneous localization and mapping (slam): Part ii. *IEEE Robotics & Automation Magazine*, 13(3):108–117, 2006.

[3] A. Bircher, M. Kamel, K. Alexis, H. Oleynikova, and R. Siegwart. Receding horizon" next-best-view" planner for 3d exploration. In *2016 IEEE international conference on robotics and automation (ICRA)*, pages 1462–1468. IEEE, 2016.

[4] A. Bircher, M. Kamel, K. Alexis, H. Oleynikova, and R. Siegwart. Receding horizon path planning for 3d exploration and surface inspection. *Autonomous Robots*, 42(2):291–306, 2018.

[5] I. Bjorling-Sachs and D. L. Souvaine. An efficient algorithm for guard placement in polygons with holes. *Discrete & Computational Geometry*, 13(1):77–109, 1995.

[6] V. Chvátal. A combinatorial theorem in plane geometry. *Journal of Combinatorial Theory*, B(18):39–41, 1975.

[7] H. Durrant-Whyte and T. Bailey. Simultaneous localization and mapping: part i. *IEEE robotics & automation magazine*, 13(2):99–110, 2006.

[8] S. K. Ghosh, J. W. Burdick, A. Bhattacharya, and S. Sarkar. Online algorithms with discrete visibility - exploring unknown polygonal environments. *IEEE Robotics Automation Magazine*, 15(2):67–76, June 2008.

[9] H. H. González-Banos and J.-C. Latombe. Navigation strategies for exploring indoor environments. *The International Journal of Robotics Research*, 21(10-11):829–848, 2002.

[10] R. Goroshin, Q. Huynh, and H.-M. Zhou. Approximate solutions to several visibility optimization problems. *Communications in Mathematical Sciences*, 9(2):535–550, 2011.

[11] L. Heng, A. Gotovos, A. Krause, and M. Pollefeys. Efficient visual exploration and coverage with a micro aerial vehicle in unknown environments. In *2015 IEEE International Conference on Robotics and Automation (ICRA)*, pages 1071–1078. IEEE, 2015.

[12] F. Hoffmann, M. Kaufmann, and K. Kriegel. The art gallery theorem for polygons with holes. In *[1991] Proceedings 32nd Annual Symposium of Foundations of Computer Science*, pages 39–48. IEEE, 1991.

[13] S. H. Kang, S. J. Kim, and H. Zhou. Optimal sensor positioning; a probability perspective study. *SIAM Journal on Scientific Computing*, 39(5):B759–B777, 2017.

[14] Y. Landa, D. Galkowski, Y. R. Huang, A. Joshi, C. Lee, K. K. Leung, G. Malla, J. Treanor, V. Voroninski, A. L. Bertozzi, Y.-H. R. Tsai, et al. Robotic path planning and visibility with limited sensor data. In *American Control Conference, 2007. ACC'07*, pages 5425–5430. IEEE, 2007.

[15] Y. Landa and Y.-H. R. Tsai. Visibility of point clouds and exploratory path planning in unknown environments. *Communications in Mathematical Sciences*, 6(4):881–913, 2008.

[16] Y. Landa, Y.-H. R. Tsai, and L.-T. Cheng. Visibility of point clouds and mapping of unknown environments. In *International Conference on Advanced Concepts for Intelligent Vision Systems*, pages 1014–1025. Springer, 2006.

[17] D. Lee and A. Lin. Computational complexity of art gallery problems. *IEEE Transactions on Information Theory*, 32(2):276–282, 1986.

[18] T. Lei and L. Ming. A robot exploration strategy based on q-learning network. In *2016 IEEE International Conference on Real-time Computing and Robotics (RCAR)*, pages 57–62. IEEE, 2016.

[19] E. Maggiori, Y. Tarabalka, G. Charpiat, and P. Alliez. Can semantic labeling methods generalize to any city? the inria aerial image labeling benchmark. In *IEEE International Geoscience and Remote Sensing Symposium (IGARSS)*. IEEE, 2017.

[20] J. O'Rourke. *Art gallery theorems and algorithms*, volume 57. Oxford University Press Oxford, 1987.

[21] J. O'Rourke and K. Supowit. Some np-hard polygon decomposition problems. *IEEE Transactions on Information Theory*, 29(2):181–190, 1983.

[22] S. Osher and R. Fedkiw. *Level set methods and dynamic implicit surfaces*, volume 153. Springer Science & Business Media, 2006.

[23] S. Osher and J. A. Sethian. Fronts propagating with curvature-dependent speed: algorithms based on hamilton-jacobi formulations. *Journal of computational physics*, 79(1):12–49, 1988.

[24] O. Ronneberger, P. Fischer, and T. Brox. U-net: Convolutional networks for biomedical image segmentation. In *International Conference on Medical image computing and computer-assisted intervention*, pages 234–241. Springer, 2015.

[25] J. A. Sethian. *Level set methods and fast marching methods: evolving interfaces in computational geometry, fluid mechanics, computer vision, and materials science*, volume 3. Cambridge university press, 1999.

[26] H. Surmann, A. Nüchter, and J. Hertzberg. An autonomous mobile robot with a 3d laser range finder for 3d exploration and digitalization of indoor environments. *Robotics and Autonomous Systems*, 45(3-4):181–198, 2003.

[27] L. Tai and M. Liu. Mobile robots exploration through cnn-based reinforcement learning. *Robotics and biomimetics*, 3(1):24, 2016.

[28] L. Tai, G. Paolo, and M. Liu. Virtual-to-real deep reinforcement learning: Continuous control of mobile robots for mapless navigation. In *2017 IEEE/RSJ International Conference on Intelligent Robots and Systems (IROS)*, pages 31–36. IEEE, 2017.

[29] Y.-H. R. Tsai, L.-T. Cheng, S. Osher, P. Burchard, and G. Sapiro. Visibility and its dynamics in a PDE based implicit framework. *J. Comput. Phys.*, 199(1):260–290, 2004.

[30] Y.-H. R. Tsai and S. Osher. Total variation and level set methods in image science. *Acta Numer.*, 14:509–573, 2005.

[31] J. Urrutia. Art gallery and illumination problems. In *Handbook of Computational Geometry*, pages 973–1027. Elsevier, 2000.

[32] L. Valente, Y.-H. R. Tsai, and S. Soatto. Information-seeking control under visibility-based uncertainty. *Journal of Mathematical Imaging and Vision*, 48(2):339–358, 2014.

[33] B. Yamauchi. A frontier-based approach for autonomous exploration. In *Computational Intelligence in Robotics and Automation, 1997. CIRA'97., Proceedings., 1997 IEEE International Symposium on*, pages 146–151. IEEE, 1997.